Lab on a Chip

PAPER

View Article Online
View Journal | View Issue

Cite this: *Lab Chip*, 2014, **14**, 3781

Microfluidic-integrated laser-controlled microactuators with on-chip microscopy imaging functionality†

Jae Hee Jung,*[ab] Chao Han,[a] Seung Ah Lee,[a] Jinho Kim[a] and Changhuei Yang[a]

Received 8th July 2014,
Accepted 24th July 2014

DOI: 10.1039/c4lc00790e

www.rsc.org/loc

The fabrication of a novel microfluidic system, integrated with a set of laser-controlled microactuators on an ePetri on-chip microscopy platform, is presented in this paper. In the fully integrated microfluidic system, a set of novel thermally actuated paraffin-based microactuators, precisely controlled by programmed laser optics, was developed to regulate flow and to provide pumping of liquid solutions without external connections. The microfluidic chip was fabricated on a complementary metal–oxide–semiconductor (CMOS)-imaging sensor chip on an ePetri platform; this configuration provided real-time, wide field-of-view, high-resolution imaging using a sub-pixel sweeping microscopy technique. The system of microactuators, which consisted of microvalves and a micropump, operated well in the microfluidic channel with a focused near-infrared laser beam providing the actuation control. As a demonstration, we used our prototype to assess cell–drug interactions and to monitor cell growth directly within an incubator in real time. The powerful combination of laser-actuated microfluidics and chip-scale microscopy techniques represents a significant step forward in terms of a simple, robust, high-throughput, and highly compact analysis system for biomedical and bioscience applications.

Introduction

"Lab on a chip (LOC)" and "micro-total analysis systems (μ-TAS)" are integrated technologies that utilize passive and active microfluidic devices to transport, manipulate, and analyze very small amounts of fluid for a variety of medical, environmental, and industrial applications. Over the past few years, microfluidic devices have shown great potential for point-of-care diagnostics, biosensors, and cell biology by providing multistage automation, parallel processing of multiple analytes, high accuracy, minimal time and energy consumption, and reconfigurability.[1–5] However, the preparation and the pre-processing of samples prior to their sensing/measurements in an assay currently require extensive biological and chemical tasks. Thus, there has been increasing interest in downscaling these functions within LOC devices and developing novel systems for preparing and detecting the tested samples "on chip". These integrated microfluidic systems would be more efficient and cost-effective, resulting in an increase in throughput and automation.

In general, a fully integrated microfluidic chip consists of many independently operating valves, pumps, and detectors to control the transport of liquid samples for complex or parallel functions. Technological development of such devices requires the miniaturization of analytical techniques and the integration of multiple microcomponents with different functionalities onto the same chip. Also, as the microfluidic systems become increasingly complicated to provide more functions, additional functional elements are required that must be integrated into the miniaturized chip. To achieve this goal, numerous efforts have led to ingenious demonstrations of on-chip microactuator (*e.g.*, valve and pump) schemes in an attempt to produce a fully integrated microfluidic chip.[6–10]

Among various microactuator approaches, paraffin-based microactuators have numerous advantages over other conventional microvalves and pumps, including a simple design, ease of fabrication, the ability to be integrated into complex microfluidic systems, and low cost.[11,12] Paraffin-based microactuators are particularly attractive for single-use, disposable microfluidic chips. Liu and coworkers developed a thermally actuated paraffin microvalve and applied it to a self-contained disposable biochip for fully integrated genetic assays.[12,13] Cho and coworkers developed a fully integrated microfluidic system for simultaneous detection of biomarkers on a lab-on-a-disk platform using disposable ferrowax microvalves.[14–17] Additionally, because the planar design of paraffin-based microactuators is simple and does not include a flexible,

[a] *Department of Electrical Engineering, California Institute of Technology, 1200 E. California Blvd., Pasadena, CA, 91125, USA*
[b] *Center for Environment, Health, and Welfare Research, Korea Institute of Science and Technology (KIST), Hwarangno 14-gil 5, Seongbuk-gu, Seoul 136-791, Republic of Korea. E-mail: jhjung@caltech.edu, jaehee@kist.re.kr*

† Electronic supplementary information (ESI) available. See DOI: 10.1039/c4lc00790e

multilayered diaphragm, such as those used in traditional actuator designs, the fabrication process of paraffin microactuators is compatible with many other material fabrication processes.[18–22] As a result, the integration of paraffin microactuators into complex microfluidic chips is less complicated than that of most conventional microactuators that involve various bulk and surface processes (*e.g.*, bulk etching of Si wafers and thin-film processing).

In previous studies of paraffin-based microactuators, an electric resistive heater has generally been used to melt the wax.[11–13,23–27] Thus, additional multilayer structures are required to accommodate the heating layer and the external electric wiring to the supply power. Recently, researchers have investigated paraffin-based, single-action microvalves that use optical heat sources, such as high-power lasers or infrared light.[14,16,28–30] The use of an optical heat source eliminates external wiring and simplifies the microfluidic-chip preparation process. This results in a simple, less expensive, single-use, disposable analysis system.

Here, we describe the implementation and the operation of a microfluidic chip integrated with laser-controlled paraffin microactuators on an on-chip microscopy platform. We show that it is possible to implement laser-controlled double-action (close/reopen) microvalves and pumps in a microfluidic system. We believe that this is the first time that both paraffin-based microvalve and micropump have been demonstrated in the same single microfluidic layer. The construction of such a microfluidic system on an on-chip microscopy platform is additionally novel. The integration of the microfluidic chip onto the complementary metal–oxide–semiconductor (CMOS) sensor enables real-time image generation of the entire microfluidic system. In addition to tracking the analytes, this combination offers a unique advantage in terms of laser control. Specifically, the built-in imaging capability allows for easy tracking of the laser and confirmation of the microactuators' actions without requiring external microscopy.

For the on-chip microscopy platform, we used our recently developed sub-pixel perspective sweeping microscopy (SPSM) technique, which demonstrated high-resolution (HR) (660 nm), wide-field (5.7 mm × 4.3 mm) imaging using a low-cost, compact-geometry configuration.[31] In SPSM, a moving illumination source creates multiple shadow images of a sample placed directly on the image sensor. These low-resolution (LR) shadow images are then processed using a pixel super-resolution algorithm to provide HR images.[31] Specifically, in our previous study, the microscope for SPSM was designed to serve as the automated self-imaging Petri dish platform (ePetri) consisting of a CMOS image sensor, light-emitting diode (LED) array illumination, and a thermoelectric cooler (TEC).[32] In a pixel super-resolution reconstruction algorithm, as the samples move farther away from the sensor (*e.g.*, due to an additional layer between the sample and the sensor), the imaging resolution deteriorates due to the diffraction of the shadows.[32] Because the laser-controlled paraffin microactuator is prepared in a transparent single-layer of the microfluidic channel, this ePetri platform can image the entire microfluidic system clearly in real-time without any barrier substance between the samples and the sensor.

In this study, using microfluidic-integrated on-chip microscopy with a laser-controlled microactuator, we demonstrated the performance of the proposed system in longitudinal drug tests of cancer cells. The system was capable of precisely controlling the microactuators in the microfluidic channel and automatically imaging the cell sample with sub-cellular resolution over a wide field of view (FOV). Our results indicated that this system would also be well suited to long-term cell-culture imaging and monitoring for biomedical and bioscience applications.

Results

System setup

Fig. 1(a) shows a schematic diagram of the entire microfluidic system, consisting of the laser focusing optics and the microfluidic-integrated image sensor (MFIIS) controlled using the ePetri platform. The input laser beam was collimated and focused and was then reflected off of a micro-electromechanical system (MEMS) mirror that was computer controlled. The reflected laser beam was then transmitted to the microactuator portion of the MFIIS chip to operate the microactuator (Fig. 1(b)). The MFIIS chip was compact, measuring approximately 10 mm × 10 mm in size, and consisted of a CMOS image sensor, a polydimethylsiloxane (PDMS) microfluidic channel layer, and a glass coverslip. This MFIIS chip was placed onto an ePetri platform for real-time, longitudinal imaging of the sample in the microfluidic chamber.

Fig. 2(a) shows a photograph of the entire system described above. Because the LED array illuminator was used for longitudinal imaging of the sample, the illuminator was separated from the ePetri platform during microfluidic actuation. Fig. 2(b) shows a schematic diagram of the laser optics. A 980 nm fiber-coupled laser (FC-980, CNI Laser, Changchun,

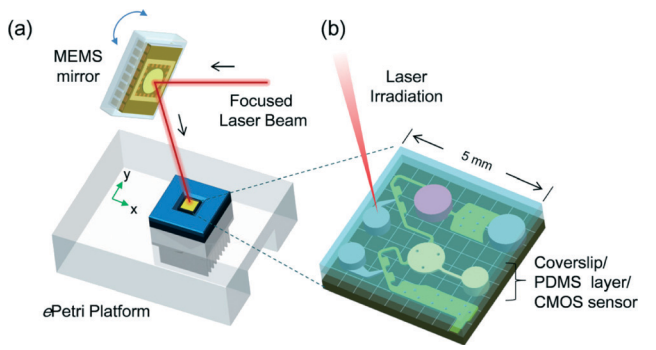

Fig. 1 Laser-actuated microfluidic ePetri system. (a) System setup. The system consists of laser-focusing optics, a micro-mirror system, and a microfluidic-integrated image sensor operated by the ePetri platform. (b) The microfluidic-integrated image sensor (MFIIS) consists of a complementary metal–oxide–semiconductor (CMOS) imaging sensor, a polydimethylsiloxane (PDMS) microfluidic layer, and a glass coverslip. All systems were controlled by a computer without the need for extra wiring or tubing.

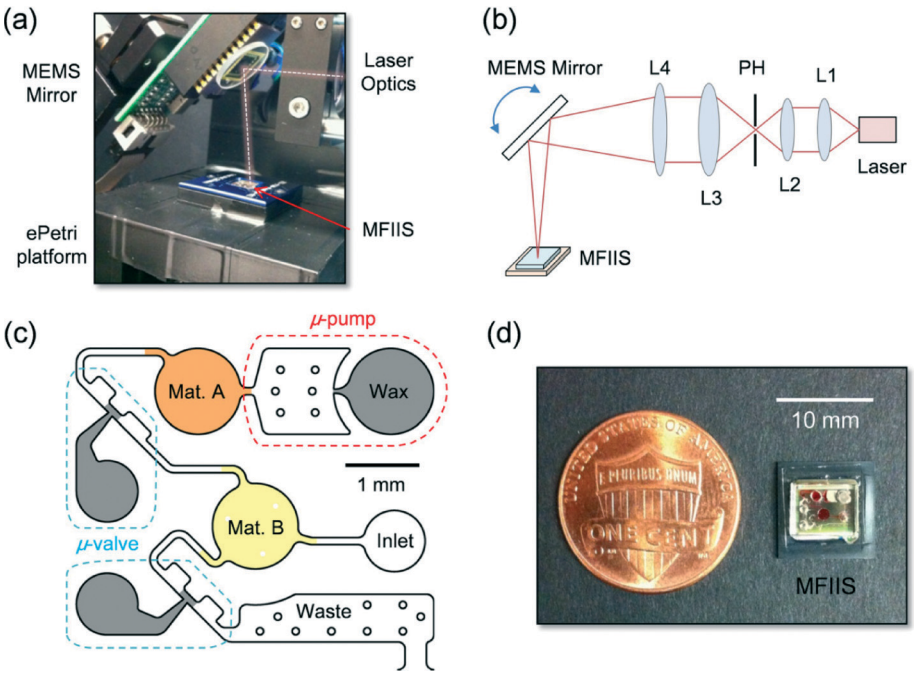

Fig. 2 (a) Photograph of the laser-actuated microfluidic ePetri with the MFIIS positioned on the ePetri platform. The white dotted line indicates the laser direction toward the MFIIS. (b) Schematic diagram of the laser optics (front view). L1: fiber collimator, f = 11 mm; L2: f = 11 mm; L3: f = 30 mm; L4: f = 75 mm; pinhole (PH): d = 30 μm. (c) Schematic diagram of the microfluidic portion of the MFIIS. The microfluidic chip consisted of a microactuator (micropump and microvalve), the phase-change material (PCM; *e.g.*, paraffin wax), chambers for Material A (*e.g.*, drug) and Material B (*e.g.*, cell suspension), and a waste zone. (d) Photograph of the actual MFIIS compared with a U.S. one-cent coin (penny). Material A and B chambers were filled with red dye so that the microfluidic chambers could be seen more clearly in the photograph.

China) was used as the optical source for microactuator control in the MFIIS chip. Using a simple lens system and a pinhole (Thorlabs Inc., Newton, NJ, USA), the focused laser beam was directed towards the MEMS mirror (S2160, Mirrorcle Technologies Inc., Richmond, CA, USA). By angularly tilting the incident laser beam using the precisely controlled MEMS mirror, we were able to laterally shift the laser beam position onto the microfluidics layer. The maximum angular tilt of the input laser beam of ~50 mrad laterally shifted the laser beam by ~5 mm on the PDMS layer. The final laser beam spot size on the MFIIS surface was ~74 μm measured at full-width half-maximum (FWHM) (Fig. S-1†).

The PDMS microfluidics were fabricated in a series of standard micromolding processes (Fig. S-2†).[33] Fig. 2(c) shows the design of the PDMS microfluidic channel, consisting of the microactuators (the micropump and microvalves), the working liquid material chambers, the inlet, and the waste zone. The entire microfluidic layer/CMOS assembly was designed simply and compactly for drug-test/cell-monitoring applications. Paraffin wax was loaded into the microvalve and micropump chambers. The details of microfluidic actuation are described in the next section. Fig. 2(d) shows a size comparison between the MFIIS chip and a United States one-cent coin (*i.e.*, a penny). The MFIIS chip was built on a commercially available CMOS image sensor; the 5.7 mm × 4.3 mm imaging area was filled with 2.2 μm pixels (Aptina MT9P031) (see Methods for more details). The microfluidic layer was bonded to the CMOS image sensor. After injection of paraffin wax and working fluid into the microactuator and the material chambers, the MFIIS chip was covered with a thin glass coverslip (CS-8S, Warner Instruments, Hamden, CT, USA; 8 mm × 8 mm, thickness: ~0.15 mm). The thin glass coverslip served to prevent evaporation of the working fluid. The MFIIS chip with a glass coverslip was then placed onto a camera board in the ePetri platform *via* a customized sensor socket for signal readout. The TEC was attached to the socket to protect target samples from the heat generated by the sensor circuit. The other side of the TEC was cooled by a central processing unit (CPU) fan.

Microfluidic experiments using a paraffin microactuator

Fig. 3 shows the "open–close–open" configuration of the paraffin microvalve; this microvalve is capable of double action and can be laser controlled to close and subsequently reopen. Each valve used a small amount of solid paraffin (76228, Sigma-Aldrich, volume: ~0.4 mm^3; melting temperature: 44–46 °C). Paraffin was loaded into each of the access holes (valve chamber) (ϕ: 0.75 mm) in the microfluidic channel using a Harris Uni-core biopsy punch (Ted Pella Inc., Redding, CA, USA). Opening or closing of the channel occurred when paraffin was melted using the heat generated by laser irradiation.

The main-flow channel was initially open. Under laser irradiation, the paraffin inside the channel melted instantaneously, and capillary force drove the molten paraffin into

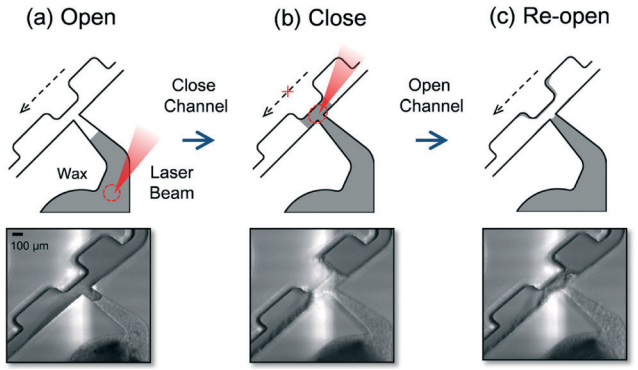

Fig. 3 Schematic diagrams and photographs of a microvalve operating under (a) open, (b) closed, and (c) reopened conditions.

the channel (Fig. 3(a)). The temperature of the air trapped inside the valve chamber also rose, resulting in a pressure increase. This increase in pressure pushed the molten paraffin into the regulated channel. Upon termination of laser irradiation, paraffin solidified in the main flow channel, resulting in a closed channel (Fig. 3(b)). The channel could be reopened by turning on the laser to initiate a rise in temperature above the melting point of paraffin; as the temperature of paraffin increased, the paraffin in the channel junction moved out of the heating zone and solidified downstream in the solidification section (Fig. 3(c)). The closing operation took place over a ~20 s period; reopening of the channel required ~60 s. The actuation of the paraffin valve required a laser power of 250–300 mW.

To demonstrate the versatility of the proposed fully integrated microfluidic system, Fig. 4 shows a schematic diagram and photographs of the device used as a single-use, disposable, simple micropump. The micropump consisted of a paraffin pump chamber, air gap chamber, and working liquid material chamber. The entire micropumping process was similar to that used for the "open–close" operation of the microvalve described above (Fig. 3(a) and (b)). First, a small amount of solid paraffin (~0.9 mm^3) was loaded into the paraffin access hole (ϕ: 1.2 mm; *i.e.*, the pump chamber). The working liquid material was introduced into the Material-A chamber using a syringe pump (Harvard Apparatus, Holliston, MA, USA) *via* an access hole. The entire microfluidic channel was then covered by a glass coverslip to seal all access holes in the microfluidic channel, including the microvalve, the micropump, and the working liquid material chambers. The working liquid retained its volume in the chamber (*i.e.*, no channel flow), because the chamber was sealed off upstream and downstream by the closed paraffin wax pump and valve (Fig. 4(a)). Note the existence of an air gap between the paraffin pump and the Material-A chamber.

To operate the paraffin micropump, first, the opening of the downstream microvalve was initiated by controlled laser irradiation. Then, the laser beam was directed to the micropump chamber to initiate micropump operation. Under laser irradiation, air trapped in the pump chamber was heated, resulting in increased pressure. This, in turn, pushed the molten paraffin into the air gap and the working liquid downstream in the microfluidic channel, as shown in Fig. 4(b), with the flow directed to the right and downwards. The micropump operation took ~60 s. The actuation of the paraffin valve required a power of 200–300 mW. The total pump capacity was ~0.27 μL. Because the pumping capacity is directly related to the paraffin-filled volume of the air gap chamber, we designed the air gap chamber with a "nozzle diffuser" geometry to reduce backflow of the molten wax in the air gap chamber after the laser was turned off.[34] During the time duration of the microactuator operation, the TEC of the ePetri platform maintained the sensor surface temperature at <30 °C.

Longitudinal cell imaging for the quantitative study of camptothecin treatment

Cell-based drug studies are an excellent longitudinal format for which a simple microfluidic system can significantly improve efficiency.[35–39] To demonstrate such an application, we performed an on-chip *in vitro* drug test with camptothecin (CPT; C9911, Sigma-Aldrich), a well-characterized anticancer drug. Because CPT is a cytotoxic quinoline alkaloid that inhibits DNA and RNA replication and synthesis by targeting the nuclear enzyme Type I topoisomerase,[40,41] it has been used successfully in cancer chemotherapy.[42] Here, we used our system to investigate HeLa cell division and migration behaviors in response to CPT.

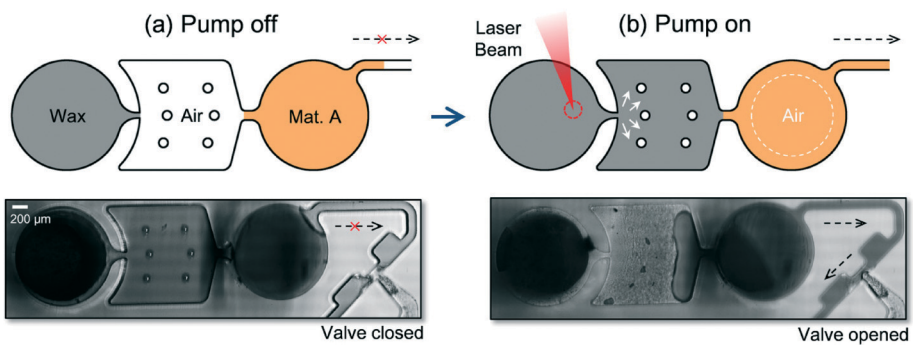

Fig. 4 Schematic diagrams and photographs of a micropump with the pump (a) off and (b) on.

Fig. 5 shows schematic diagrams and photographs of the microfluidic procedures used for the drug test. The microfluidic channel, consisting of cell and drug chambers, two paraffin microvalves, one micropump, and a waste chamber, is shown in Fig. 5(a). After loading the paraffin into the micropump and microvalve chambers, the first microvalve (Microvalve-1) was closed (Fig. 5(a)). The cell suspension and drug were then injected into each chamber using a syringe pump. The entire PDMS microfluidic layer was then sealed using a glass coverslip. To attach cells onto the CMOS sensor surface, the ePetri platform was placed inside a humidified 5% CO_2 incubator at 37 °C for ~2 h (Fig. 5(b)). Microvalve-1 was then reopened using a micropump to allow the drug to flow into the cell chamber (Fig. 5(c)). Finally, when the drug filled the cell chamber, after pushing the cell medium to the waste zone, Microvalves-1 and -2 were closed sequentially, and the ePetri platform was assembled with the LED illumination array. The ePetri platform initiated longitudinal cell imaging for drug testing (Fig. 5(d)). During time-lapse cell monitoring, no leakage was observed in the cell chamber. Before the experiment, we treated the channel and the sensor surface using the procedure detailed in the Methods section. During the entire experimental procedure, the MFIIS chip was placed on the TEC of the ePetri platform. The cells were cultured in the cell chamber in the microfluidic layer (diameter: 1.2 mm; height: 160 μm). In the CO_2 incubator, the TEC (7.7 W) was turned on to prevent the sensor surface temperature from exceeding 37 °C during imaging (Fig. S-3†).

We imaged HeLa cells on the ePetri platform using the SPSM technique to demonstrate the ability of the platform to image confluent cell samples. Fig. 6 shows bright-field images of living HeLa cells taken using the ePetri platform. Fig. 6(b) shows a raw image from a small region of Fig. 6(a) with the entire FOV. The LR image from a small region of Fig. 6(b) is shown in Fig. 6(c). A sequence of LR images was obtained by sweeping the LED illumination using an incremental tilt/shift process. A shift-and-add pixel super-resolution algorithm was applied to reconstruct a single HR image (Fig. S-4†).[31] This algorithm shifted each LR image by the relative sub-pixel shift given by the computed illuminator position vector and then added them together to fill a blank HR image grid with an enhancement factor of n, where each ($n \times n$) pixel area of the HR image grid corresponded to a

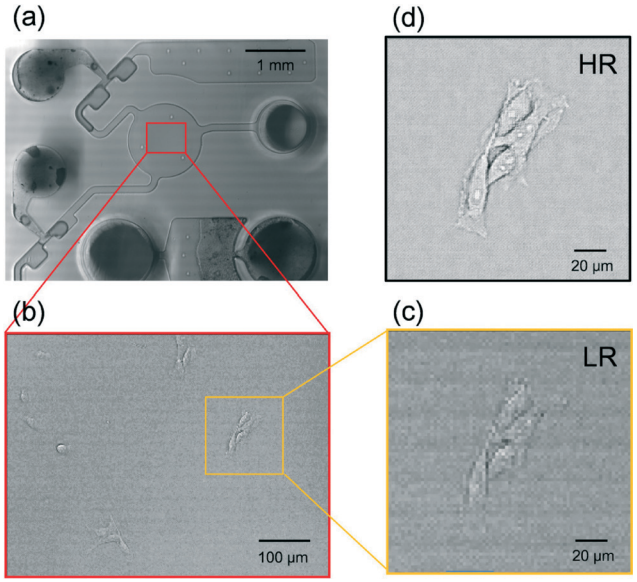

Fig. 6 Bright-field images of living HeLa cells taken with an ePetri sensor chip. (a) Wide field-of-view (FOV) images of the entire microfluidic chip. (b) Bright-field images of the area highlighted in (a). (c) Low-resolution (LR) image. (d) Reconstructed high-resolution (HR) image of the area highlighted in (b).

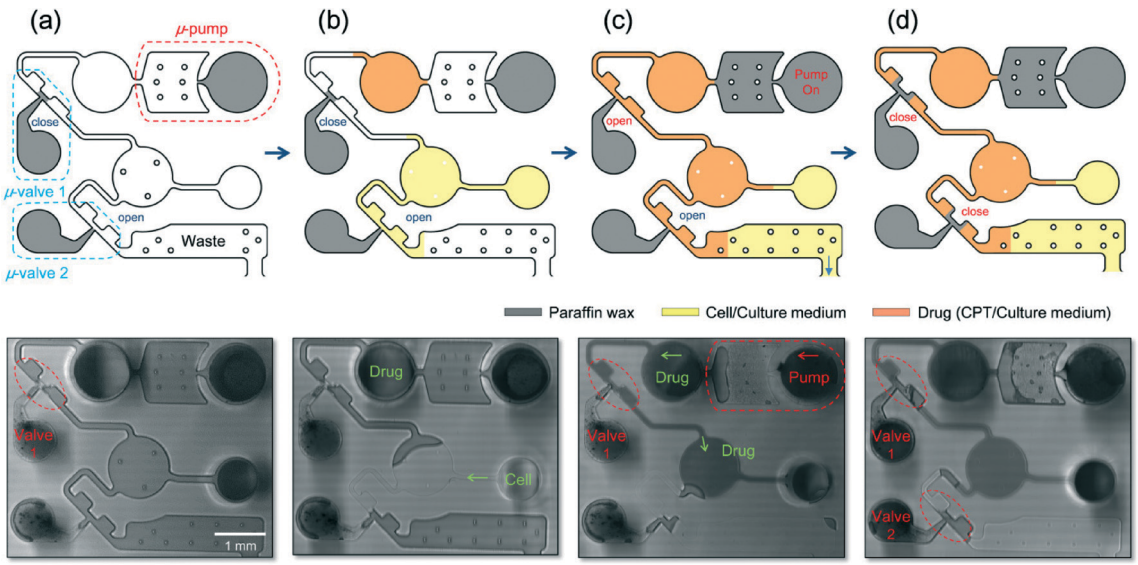

Fig. 5 Drug-testing procedure: (a) loading of the wax with Valve-1 closed, (b) loading of the cell suspension and drug, and covering the microfluidic chip with a glass coverslip, (c) after ~2 h of pre-incubation, opening of Valve-1 and turning the pump on, and (d) closing of Valves-1 and -2, and initiation of longitudinal cell monitoring.

single (1 × 1) pixel area of the LR image grid. Fig. 6(d) shows the reconstructed HR image of Fig. 6(c), which has an enhancement factor of 8. From the reconstructed HR image, the center and the boundary of HeLa cells were clearly resolved compared with those of the LR image. The ePetri platform collected microscopy resolution images over the entire area of the sensor, providing a wide FOV that was orders of magnitude higher than the FOV of a conventional microscope with comparable resolution. More details of the ePetri platform using SPSM were described in our previous studies.[31,32]

In this longitudinal drug study, we prepared two cell culture groups: the CPT treatment group and a control group. Using the drug test procedure described above, a cell-culture medium with 1 μM CPT was loaded into the microfluidic culture chamber after 0 or 6 h of incubation. The control group was also loaded with the culture medium without CPT. Fig. 7 shows the reconstructed HR time-lapse images of the cells

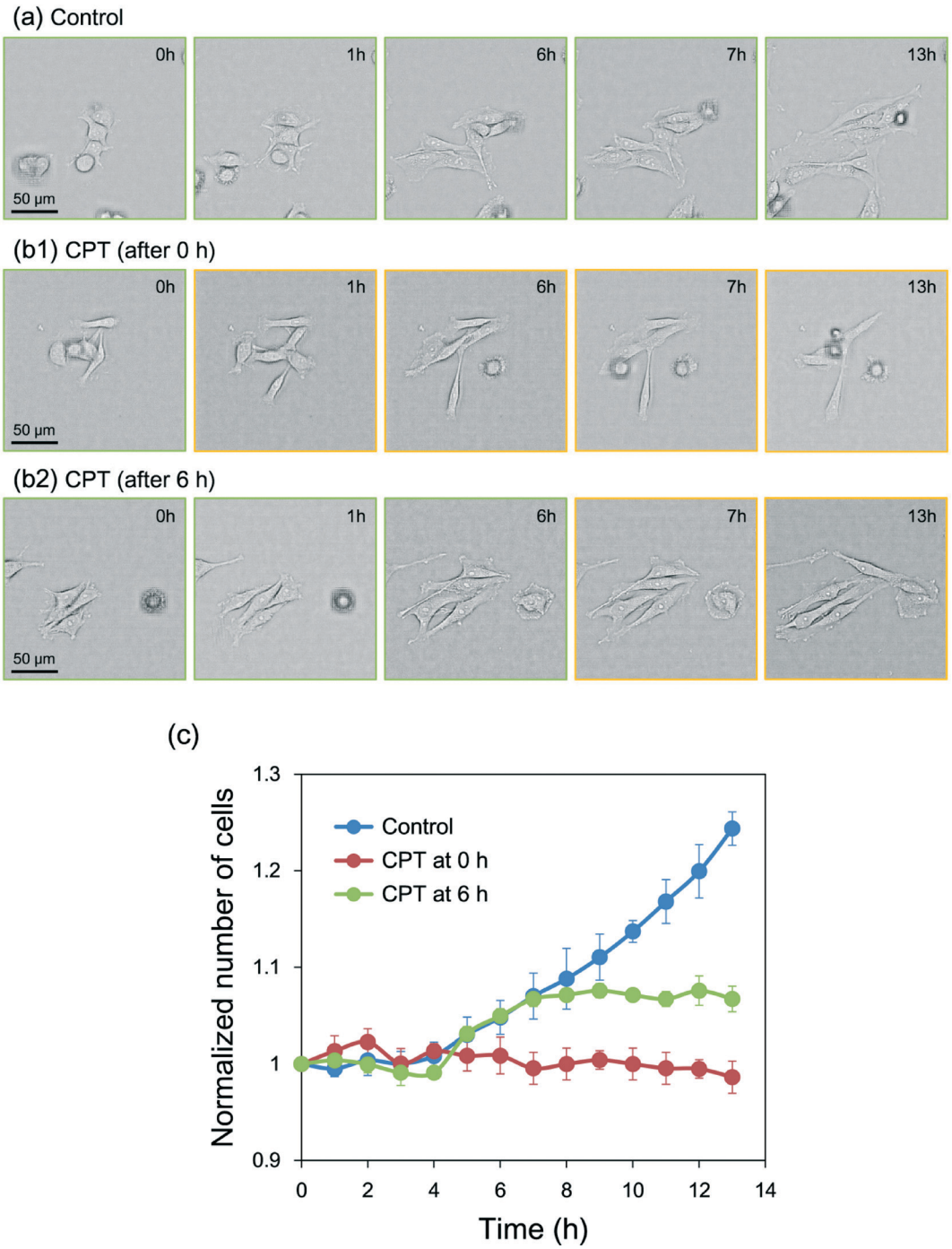

Fig. 7 Long-term monitoring of living cells undergoing camptothecin (CPT) treatment (1 μM): (a) the control group, (b) the CPT groups after drug injection at 0 h (b1) and at 6 h (b2), and (c) the cell count over time for the control and CPT groups (n = 3).

from a specific sublocation as a result of the CPT treatment. To demonstrate the longitudinal cell variation, a sequence of images was acquired at 1 h intervals over a 13 h period. Based on time-lapse imaging data, we were able to detect and track the variation of individual cells in space and time. Both the control (Fig. 7(a)) and the CPT group (Fig. 7(b)) showed a clear cell shape. However, after drug injection by microfluidic actuators, the growth of cells was slowed down by CPT and finally stopped, whereas cells in the control group kept growing by division over time. The migration of the cells in the CPT group also decreased, and their cell growth eventually stopped over the course of time-lapse imaging (Movie S-1†). Fig. 7(c) shows the variation in the normalized number of cells in the control and CPT groups. At 0 h, the control and CPT groups had 72 ± 13 and 54 ± 15 cells, respectively. At 13 h, the cell count for the control group increased by 24.4 ± 1.73%, while the cell count for the CPT group (by treatment at 0 h) retained close to its initial value (−1.4 ± 1.33%) (Fig. 7(c)). In the case of another CPT group, the cell count slowly increased by 7.6 ± 0.72% up to the 6 h point, at which time CPT was injected; the cell count reached 6.7 ± 1.67% at the end of 13 h. From these data, we can conclude that CPT inhibited cell proliferation and migration and that the microfluidic-integrated ePetri system can be used for automated drug testing and cell behavior analyses.

Discussion

In this study, we demonstrated a fully integrated microfluidic on-chip microscopy system that used a system of laser-controlled paraffin microactuators and an ePetri microscopy platform by an SPSM HR-imaging technique. The paraffin-based microactuators demonstrated good performance under precisely controlled laser-beam actuation; moreover, the CMOS image sensor used by the substrate imaged the entire microfluidic system in real time. It is also worth noting that despite our need to position the laser with submillimeter precision, the actual alignment of the microfluidic system with the laser is not critical as the image sensor provides a robust method of tracking and ensuring that the laser is at the desired location within ~10 μm precision. In general, previous studies related to the microactuator with optical heating sources used a beam positioning system (*e.g.*, a digital mirror)[43–45] or a mechanical moving-stage system (*e.g.*, an *x*–*y* moving stage or a centrifugal disk platform)[14,15,29,46] for the interaction of the light beam with the target. Compared with previous beam positioning/moving-stage systems, the current optics system (including the MEMS mirror and the laser diode) may be less expensive, more compact, and simpler to use. Finally, the ePetri platform provided longitudinal live-cell imaging and reconstructed HR images of the cells. From the fluidic and drug experiments, the fully integrated system appeared to be robust and exhibited suitable performance for its purpose. Additionally, the implementation of laser-controlled double-action microvalves and pumps is a novel development and showcases the versatility of using laser manipulation to implement complex actuation microfluidic sequences.

Although the response time of these microactuators is relatively slow compared with most conventional microvalves and micropumps (~1 ms), the paraffin-based actuators may be useful in many microfluidic applications in which a rapid response is not critical. The time response of a paraffin-based microactuator is dependent largely on the temperature ramping rate resulting from laser irradiation, 2–4 °C s^{-1} in our experiments, as well as on the thermal mass and thermal conductivity of paraffin wax. The response time could possibly be improved by adding absorbing dyes to the wax to increase the absorptivity of the wax with respect to incident laser irradiation or by focusing the incident laser beam to a smaller spot size to increase laser power.[26,28] Additionally, a phase-transition material with a lower melting temperature could be used. In this study, each microactuator in the experiment operated in sequence due to the use of a single laser beam. However, if multipoint laser irradiation was used (*e.g.*, *via* a computer-controlled digital mirror device) for simultaneous regulation of individual microactuators,[43] then the entire microactuator operation could be reduced.

According to the study by Park and coworkers, the maximum holding pressure of their ferrowax microvalves was ~400 kPa.[28] Pal and coworkers reported that no leakage was observed from the paraffin-based microvalve up to ~1700 kPa.[11] In addition, Liu and coworkers demonstrated that the paraffin-based microvalves had zero leakage in a "closed" position with a maximum hold-up pressure of ~270 kPa.[13] When we loaded two target material types (*e.g.*, the cell suspension and the drug) into the microfluidic chip, only the initial dropping (<1.2 μL) of the target material into the specific microfluidic chamber was required (*i.e.*, no need for extra tubing connections with high-pressure differentials). In this case, the theoretical maximum pressure applied to the microvalve would be <0.7 kPa, which is >350-fold lower than the holding pressure cited in the previous literature. Although this study did not provide specific information on the maximum pressure capabilities of the microvalve used, the proposed paraffin-based microvalve had sufficient holding pressure and functioned well under the microfluidic conditions presented. Also, during time-lapse cell monitoring (>13 h) after the microactuation of the valve, no leakage was observed in any of the chambers.

In the drug test performed in this study, the microfluidics demonstrated was designed to assay a single drug in a single cell type due to the limited size of the CMOS sensor substrate. However, this technique could easily be scaled to larger CMOS sensor substrates to accommodate a larger PDMS channel layer with various microfluidic functions. As another approach to increasing functionality, if precise loading of paraffin material (*e.g.*, on the order of picoliters) into each microactuator chamber is achieved using a computer-controlled wax injector (Microdrop GmbH, Germany), then additional microactuators could be activated in the current microfluidic layer due to the reduced microactuator size.

Furthermore, the use of a precision wax injector could eventually lead to a manufacturing method for paraffin microactuators in microfluidic devices. It is also worth noting that this microactuator is not limited to paraffin and can be extended to many other materials that can undergo phase transition from a solid to a liquid in response to changes in temperature.

Conclusion

In this study, a laser-actuated microfluidic on-chip microscopy system that utilizes fully integrated microactuators on an ePetri platform was demonstrated. A set of thermally activated, laser beam-controlled paraffin microactuators was integrated into the microfluidic chip. Fluidic experiments indicated that these microactuators were robust and easy to integrate into functional microfluidic devices. As an application of this system, the drug test experiment demonstrated that the proposed laser-controlled paraffin-based microactuator system was compatible with the assay and easily integrated into real-time on-chip microscopy with an ePetri platform. This light-actuated microfluidic ePetri system also allowed monitoring of longitudinal cell variations at high resolution. We believe that this microfluidic integrated on-chip microscopy technique can potentially play a significant role in the rapid diagnosis or point-of-care analysis for the detection of pathogens/diseases using microfluidic biochemical treatments or drug screening, with high throughput and rapid results for biomedical and bioscience applications.

Methods

Fabrication of the microfluidic-integrated imaging sensor (MFIIS)

The microfluidic-integrated image sensor (MFIIS) comprised two parts: a CMOS image sensor and a PDMS microfluidic channel. The two parts were fabricated separately and then assembled. We used an MT9P031 image sensor (2.2 μm pixels, Aptina). The glass cover was removed from each sensor by cutting the edges of the glass on a hot plate (180 °C). The microlens layer was removed by treating the sensor under oxygen plasma for 10 min (120 W) to provide direct access to the sensor pixels. The PDMS microfluidic channel, fabricated using a standard soft-lithography procedure, was bonded to the image sensor after oxygen plasma treatment (40 W, 30 s) (Fig. S-2†). The diameters of the microvalve and micropump chambers were 0.75 and 1.2 mm, respectively. The diameter of each working liquid material chamber was 1.2 mm. The height of the channel was ~160 μm, and the thickness of the PDMS microfluidic chip was ~1.4 mm. The channel width was 100 μm, except for the channel between the pump and the air gap chamber (70 μm). After the experiment, the image sensors were reused after cleaning with deionized water in an ultrasonic bath for 30 s at 70 °C.

Temperature measurements

For measuring the local temperature inside the microfluidic device during laser-controlled microactuator operation and imaging process, a 76 μm-diameter T thermocouple (Omega Engineering) was inserted into the cell-culture chamber, and the temperature was measured by a digital thermometer.

Microfluidic cell culture and time-lapse imaging

HeLa cells were first cultured in Dulbecco's modified Eagle's medium (DMEM, Invitrogen), supplemented with L-glutamine (4 mM; Gibco), 1% (v/v) penicillin–streptomycin (Gibco), and 10% (v/v) fetal bovine serum (FBS; Gibco) in culture dishes and maintained under a 5% CO_2 humidified atmosphere at 37 °C. DMEM was also used for dilution of CPT (1 μM). To promote cell adhesion, the CMOS surfaces of the MFIIS chips were treated with poly-L-lysine (0.01%, Sigma-Aldrich) for 15 min and washed three times with distilled water. During the logarithmic growth period, cells were harvested by trypsin (0.05%, Invitrogen) and resuspended in DMEM. For the experiment, the cell solution was adjusted to a concentration of 5×10^6 cells per milliliter and loaded into the cell chamber of the microfluidic device. After ~2 h of incubation to permit the cells to attach to the image sensor surface, the image sensor was mounted onto the socket of the ePetri platform. Finally, the MFIIS was covered with a coverslip.

Acknowledgements

This research was supported by the National Institutes of Health under grant no. 1R01AI096226-01 and in part by the KIST Institutional Program (2E24652).

References

1 L. Dong and H. Jiang, *Soft Matter*, 2007, **3**, 1223–1230.
2 G. M. Whitesides, *Nature*, 2006, **442**, 368–373.
3 T. M. Squires and S. R. Quake, *Rev. Mod. Phys.*, 2005, **77**, 977.
4 D. Janasek, J. Franzke and A. Manz, *Nature*, 2006, **442**, 374–380.
5 D. Psaltis, S. R. Quake and C. Yang, *Nature*, 2006, **442**, 381–386.
6 K. W. Oh and C. H. Ahn, *J. Micromech. Microeng.*, 2006, **16**, R13.
7 D. Laser and J. Santiago, *J. Micromech. Microeng.*, 2004, **14**, R35.
8 C. Zhang, D. Xing and Y. Li, *Biotechnol. Adv.*, 2007, **25**, 483–514.
9 B. D. Iverson and S. V. Garimella, *Microfluid. Nanofluid.*, 2008, **5**, 145–174.
10 A. K. Au, H. Lai, B. R. Utela and A. Folch, *Micromachines*, 2011, **2**, 179–220.
11 R. Pal, M. Yang, B. N. Johnson, D. T. Burke and M. A. Burns, *Anal. Chem.*, 2004, **76**, 3740–3748.
12 R. H. Liu, J. Yang, R. Lenigk, J. Bonanno and P. Grodzinski, *Anal. Chem.*, 2004, **76**, 1824–1831.

13 R. H. Liu, J. Bonanno, J. Yang, R. Lenigk and P. Grodzinski, *Sens. Actuators, B*, 2004, **98**, 328–336.
14 J. Park, V. Sunkara, T.-H. Kim, H. Hwang and Y.-K. Cho, *Anal. Chem.*, 2012, **84**, 2133–2140.
15 B. S. Lee, Y. U. Lee, H.-S. Kim, T.-H. Kim, J. Park, J.-G. Lee, J. Kim, H. Kim, W. G. Lee and Y.-K. Cho, *Lab Chip*, 2011, **11**, 70–78.
16 B. S. Lee, J.-N. Lee, J.-M. Park, J.-G. Lee, S. Kim, Y.-K. Cho and C. Ko, *Lab Chip*, 2009, **9**, 1548–1555.
17 Y.-K. Cho, J.-G. Lee, J.-M. Park, B.-S. Lee, Y. Lee and C. Ko, *Lab Chip*, 2007, **7**, 565–573.
18 P. Selvaganapathy, E. Carlen and C. Mastrangelo, *Sens. Actuators, A*, 2003, **104**, 275–282.
19 H. Jerman, *J. Micromech. Microeng.*, 1994, **4**, 210.
20 M. A. Unger, H.-P. Chou, T. Thorsen, A. Scherer and S. R. Quake, *Science*, 2000, **288**, 113–116.
21 R. C. Anderson, X. Su, G. J. Bogdan and J. Fenton, *Nucleic Acids Res.*, 2000, **28**, e60.
22 E. Lagally, I. Medintz and R. Mathies, *Anal. Chem.*, 2001, **73**, 565–570.
23 E. T. Carlen and C. H. Mastrangelo, *J. Microelectromech. Syst.*, 2002, **11**, 408–420.
24 B. Yang and Q. Lin, *Sens. Actuators, A*, 2007, **134**, 194–200.
25 X. Weng, H. Jiang, J. Wang, S. Chen, H. Cao and D. Li, *J. Micromech. Microeng.*, 2012, **22**, 075003.
26 K. W. Oh, K. Namkoong and C. Park, *Proc. microTAS*, 2005, pp. 554–556.
27 E. T. Carlen and C. H. Mastrangelo, *J. Microelectromech. Syst.*, 2002, **11**, 165–174.
28 J.-M. Park, Y.-K. Cho, B.-S. Lee, J.-G. Lee and C. Ko, *Lab Chip*, 2007, **7**, 557–564.
29 K. Abi-Samra, R. Hanson, M. Madou and R. A. Gorkin III, *Lab Chip*, 2011, **11**, 723–726.
30 G. Chen, F. Svec and D. R. Knapp, *Lab Chip*, 2008, **8**, 1198–1204.
31 G. Zheng, S. A. Lee, Y. Antebi, M. B. Elowitz and C. Yang, *Proc. Natl. Acad. Sci. U. S. A.*, 2011, **108**, 16889–16894.
32 S. A. Lee, J. Erath, G. Zheng, X. Ou, P. Willems, D. Eichinger, A. Rodriguez and C. Yang, *PLoS One*, 2014, **9**, e89712.
33 D. C. Duffy, J. C. McDonald, O. J. Schueller and G. M. Whitesides, *Anal. Chem.*, 1998, **70**, 4974–4984.
34 J.-H. Tsai and L. Lin, *J. Microelectromech. Syst.*, 2002, **11**, 665–671.
35 C. Han, S. Pang, D. V. Bower, P. Yiu and C. Yang, *Anal. Chem.*, 2013, **85**, 2356–2360.
36 T. Preckel, G. Luedke, S. D. Chan, B. N. Wang, R. Dubrow and C. Buhlmann, *JALA*, 2002, **7**, 85–89.
37 M. J. Kim, S. C. Lee, S. Pal, E. Han and J. M. Song, *Lab Chip*, 2011, **11**, 104–114.
38 Y.-C. Toh, T. C. Lim, D. Tai, G. Xiao, D. van Noort and H. Yu, *Lab Chip*, 2009, **9**, 2026–2035.
39 M.-H. Wu, S.-B. Huang and G.-B. Lee, *Lab Chip*, 2010, **10**, 939–956.
40 Y.-H. Hsiang, R. Hertzberg, S. Hecht and L. Liu, *J. Biol. Chem.*, 1985, **260**, 14873–14878.
41 A. G. Schultz, *Chem. Rev.*, 1973, **73**, 385–405.
42 R. Garcia-Carbonero and J. G. Supko, *Clin. Cancer Res.*, 2002, **8**, 641–661.
43 Y. Shirasaki, M. Tatsuoka, M. Yamagishi, J. Mizuno, S. Shoji and T. Funatsu, *J. Sens.*, 2013, **2013**, 436492.
44 H. Sugino, K. Ozaki, Y. Shirasaki, T. Arakawa, S. Shoji and T. Funatsu, *Lab Chip*, 2009, **9**, 1254–1260.
45 Y. Shirasaki, J. Tanaka, H. Makazu, K. Tashiro, S. Shoji, S. Tsukita and T. Funatsu, *Anal. Chem.*, 2006, **78**, 695–701.
46 M. Krishnan, J. Park and D. Erickson, *Opt. Lett.*, 2009, **34**, 1976–1978.